Journal of Alloys and Compounds 515 (2012) 90–95

Contents lists available at SciVerse ScienceDirect

Journal of Alloys and Compounds

journal homepage: www.elsevier.com/locate/jallcom

Electrochemical characterization with homopolymer of 2-propen-1-amine coating on artificial graphite/carbon/silicon composites as anode materials for lithium ion batteries

Tzoo-Shing Yeh [a], Yu-Shiang Wu [b,*], Yuan-Haun Lee [a]

[a] Department of Material Science and Engineering, National Taiwan University, Taipei, 106 Taiwan, ROC
[b] Department of Mechanical Engineering, China University of Science and Technology, Taipei, 115 Taiwan, ROC

ARTICLE INFO

Article history:
Received 5 May 2011
Received in revised form
16 November 2011
Accepted 21 November 2011
Available online 28 November 2011

Keywords:
Lithium-ion batteries
Anode materials
Composite
Cycling stability

ABSTRACT

This study reports the coating of spherical artificial graphite/disordered carbon/silicon (AG/C/Si) with a homopolymer of 2-propen-1-amine (PAA) layer. Transmission electron microscopy (TEM) observations clearly showed that the surface of the particle was coated with an amorphous layer of PAA-coated AG/C/Si composites. The resulting PAA-coated AG/C/Si electrode structure did not destroy locally because of large volume change. For both charge and discharge at 0.1 C, the PAA-coated AG/C/Si yielded the first columbic efficiency of approximately 89.1% and the first irreversible capacity decreased from 95.1 to 55.0 mAh g^{-1}. Moreover, the discharge capacity was 410.1 mAh g^{-1} after 50 cycles, and its capacity retention increased to 91.5%. The addition of PAA decreased the specific surface area (BET) of the AG/C/Si composites and reduced the direct contact between the anode electrode surface and the electrolyte. These results indicate that PAA-coated AG/C/Si composites have relatively lower electrochemical resistance and favorable cycling stability.

1. Introduction

This study sought to improve the reversible capacity and lower the first irreversible capacity of the anode materials of lithium ion batteries. Most current commercial lithium-ion batteries use graphite as the anode material. Because of global energy and environmental considerations, transportation vehicles use energy storage batteries as the main power source. Lithium-ion batteries are an ideal high-capacity, high-power energy source. Artificial graphite is superior to natural graphite as a high-power anode material [1,2]. However, the capacity of artificial graphite is approximately 340 mAh g^{-1}, and researchers are currently searching for higher-capacity anode materials. Currently, silicon is the most attractive candidate of all known materials because of its theoretical capacity. Because of their extremely high capacity, up to 4200 mAh g^{-1}, alloys with a maximal Li content can form $Li_{22}Si_5$ in Li–Si systems [3,4]. Unfortunately, two obstacles prevent the use of silicon in commercial applications. First, silicon has poor cyclability because of drastic volume changes between its delithiated and lithiated states; the difference in volume between the delithiated silicon and fully lithiated $Li_{22}Si_5$ phases is approximately 300% [5–7]. This creates internal cracks in the structure, causing dramatic morphological changes. Second, the first cycle has higher irreversible capacity because of phase transformation. Great efforts have been made to improve the cycling performance of silicon in the previous few years. Preparing silicon-based materials with a designed nanostructure and carbon–silicon composite seems to be a possible way to solve this problem [8–14]. Nanostructured materials usually exhibit a large pore volume that allows the digestion of considerable volume expansion without causing mechanical fracture or cracking [15]. This architecture can accommodate the large volume change during lithium insertion/extraction. Particular porous Si-based anode materials can effectively alleviate the volume expansion [16]. Additional nanosized Si composites have been prepared via ball-milling technique using various Si sources [17–19]. By contrast, carbon of the C/Si composite materials can buffer the volume expansion and enhance the electronic conductivity [20–25]. The buffer matrix can effectively reduce the volume expansion of metal oxide during the lithium intercalation, preventing mechanical failure and resulting in improved cycle life [26–33]. Combining nanostructures and carbon composites is practical for enhancing the electrochemical performance of silicon. Homopolymer of 2-propen-1-amine is generally stable in common organic electrolyte, and quite suitable as a coating shell to protect the anode materials. This homopolymer contains an amino group (NH_2), and the nitrogen atoms contain a lone pair of electrons that can behave as potential sites for the complexation of

* Corresponding author at: 245, Sec.3, Yen-Chiu-Yuan Road, Nankang, Taipei 115, Taiwan, ROC. Tel.: +886 2 27867048x37; fax: +886 2 27867253.
E-mail address: yswu@cc.cust.edu.tw (Y.-S. Wu).

0925-8388/$ – see front matter © 2011 Elsevier B.V. All rights reserved.
doi:10.1016/j.jallcom.2011.11.089

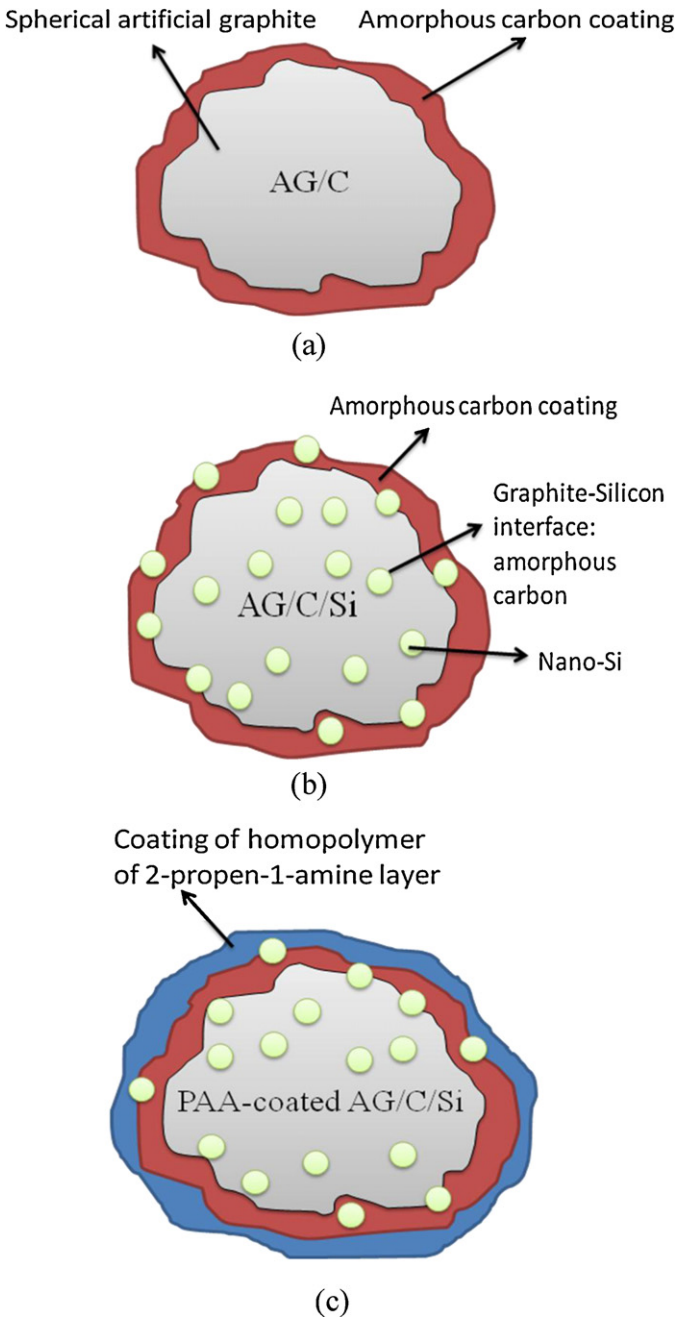

Fig. 1. Schematic illustration of the preparation of the composite materials: (a) sample AG/C, (b) sample AG/C/Si, and (c) sample PAA-coated AG/C/Si.

lithium salts to the polymer, increasing the lithium ion conduction.

This study investigates a new method for coating an artificial graphite/silicon composite material at a low temperature to create an anode material for high-capacity lithium ion batteries. The proposed homopolymer of 2-propen-1-amine matrix provides excellent cycling stability and columbic efficiency.

2. Experimental

2.1. Sample preparation

Artificial graphite flakes (D50: 15 μm, 99.9%) were prepared using 30 μm spherical powders and a jet milling process developed in China. The nano-Si powder (50 nm, >98%,) and homopolymer of 2-propen-1-amine were obtained from Aldrich Co. (USA) and Nitto Boseki Co. (Japan), respectively. Fig. 1(a) and (b) shows schematic diagrams of the artificial graphite/disordered carbon (AG/C) composite

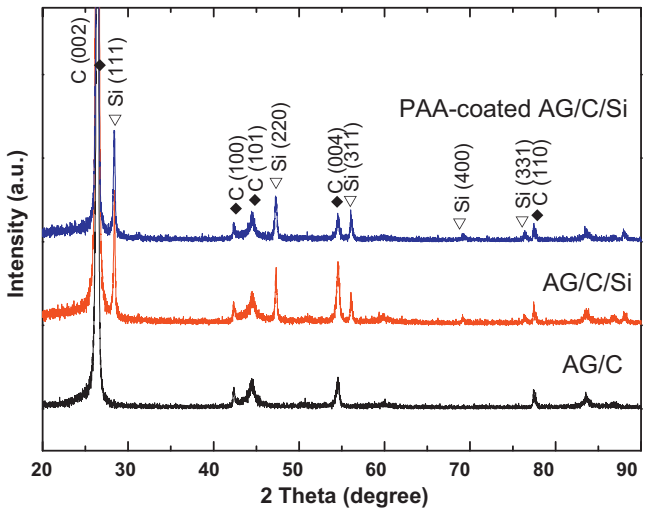

Fig. 2. XRD patterns of the composite materials.

materials with a weight ratio of 20:4 and artificial graphite/disordered carbon/silicon (AG/C/Si) with a weight ratio of 20:3:4. The petroleum pitch was dissolved in acetone solvent. Nano-Si and spherical artificial graphite were introduced to the solution and homogeneously mixed in a slurry. To obtain a solid state, the acetone solvent was evaporated while stirring the mixture at 60 °C, followed by a heating process. The precursor powders were placed on an alumina boat and fired at 1000 °C for 1 h in the heat-treatment furnace filled with an argon atmosphere at a heating rate of 5 °C min^{-1}. After the mixture was pyrolyzed, the AG/C and AG/C/Si composites formed as the mixture cooled to room temperature. The AG/C and AG/C/Si composites were then sieved using a 400-mesh sifter.

Fig. 1(c) shows a schematic diagram of the PAA-coated AG/C/Si composite materials. The weight ratio of the mixed AG/C/Si and homopolymer of 2-propen-1-amine was 9:1. The homopolymer of 2-propen-1-amine was dissolved in DI water used as solvent. The AG/C/Si was introduced to the PAA solution and homogeneously mixed in a slurry. The beaker was maintained at 80 °C under stirring until the solvent evaporated. The resulting powder was collected and dried at 100 °C for 12 h.

2.2. Structure characterization

Sample morphology was observed using scanning electron microscope (SEM, Philips XL30) and field emission scanning electron microscope (FE-SEM, Jeol JSM-6500F). The specific surface areas of the samples were measured using a BET specific surface area analyzer (BET, Micrometry Tristar 3000) based on the adsorption isotherm of N_2 at 77 K. Powder X-ray diffraction (XRD, Rigaku TTRAX 3) measurements were performed using Cu Kα radiation to identify the material's crystalline phase. The morphology and particle size of the composite materials were observed under a high resolution transmission electron microscope (TEM, Philips TECNAI F20 G2).

2.3. Electrochemical characterization

This study conducted charge/discharge capacity tests for anode materials fabricated as coin-type cells. The anode electrodes were prepared using 90 wt.% active materials and 10 wt.% polyvinylidene fluoride (PVdF) as a binder. These materials were mixed homogeneously with N-methylpyrrolidone (NMP) for 30 min to obtain a slurry with the desired viscosity. A copper foil 14 μm thick was coated with the slurry and heated at 150 °C until the NMP solvent evaporated entirely. The coated film was then cut into 13 mm diameter circles. The cathode electrode material was lithium metal. The electrolyte solution was 1 M $LiPF_6$/ethylene carbonate (EC) + ethylmethyl carbonate (EMC) + dimethyl carbonate (DMC) (1:1:1 by volume). Electrode tests were conducted at room temperature to determine the charge and discharge measurements (Arbin, BT 2000). The cells were galvanostatically charged and discharged at 0.1 C-rates between the cut-off voltage of 0.005 and 2 V. The AC impedance spectrum was recorded using an impedance analyzer (Solartron, 1260) at a 10^{-2}–10^{6} Hz frequency range.

3. Results and discussion

3.1. Sample characterization

Fig. 2 displays the XRD patterns of the samples. The AG/C exhibited a sharp (0 0 2) graphite diffraction peak, while AG/C/Si exhibited the crystalline diffraction peaks of graphite and silicon.

Table 1
The first charge/discharge capacities and the capacity retentions after 50 cycles.

Sample	First charge capacity ($mAh\,g^{-1}$)	First discharge capacity ($mAh\,g^{-1}$)	First[a] irreversible capacity ($mAh\,g^{-1}$)	First[b] columbic efficiency (%)	50th discharge capacity ($mAh\,g^{-1}$)	Capacity[c] retentions after 50 cycles (%)	BET ($m^2\,g^{-1}$)
AG/C	360.5	329.2	31.3	91.3	299.7	91.0	1.9
AG/C/Si	570.7	475.6	95.1	83.3	360.0	75.7	4.1
PAA-coated AG/C/Si	503.3	448.3	55.0	89.1	410.1	91.5	2.7

[a] First irreversible capacity ($mAh\,g^{-1}$)=First charge capacity − First discharge capacity.
[b] First columbic efficiency (%) = 100% − ((First irreversible capacity/First charge capacity) × 100%).
[c] Capacity retentions after 50 cycles (%) = (50th discharge capacity/First discharge capacity) × 100%.

However, the AG/C/Si composites exhibited no SiO_2 or SiC crystalline phases. By contrast, the C (0 0 2) and Si (1 1 1) peak intensity became weaker when coated with PAA. Fig. 3(a) and (b) shows FE-SEM images of the spherical artificial graphite (AG) and carbon coated spherical artificial graphite (AG/C). The AG/C sample surface became smoother than the spherical artificial graphite. This finding is consistent with the BET results, as Table 1 shows. Fig. 3(c) displays that in the AG/C/Si sample, nano-Si was normally distributed in a graphite matrix, creating a buffer during the insertion/extraction of lithium ions. Fig. 3(d) shows that in the PAA-coated AG/C/Si composites, the particles became more agglomerated. The TEM observations in Fig. 4(a) and (b) indicate that the nano-Si exhibited an average particle size of approximately 5–100 nm, and the spherical artificial graphite particles coated by the amorphous carbon from pitch (AG/C). Fig. 4(c) shows the AG/C/Si composites. Fig. 4(d) and (e) clearly indicates that the surface of the particle is coated with an amorphous layer in PAA-coated AG/C/Si composites. These TEM results confirm that the PAA layer is coated on the AG/C/Si composites. The AG/C/Si and PAA-coated AG/C/Si composites sample on the carbon-coated grid for the TEM measurement was directly subjected to EDX measurement, as shown in Fig. 5(a) and (b). PAA coating reduces the oxygen content of composites significantly. Therefore, PAA coating can help reduce the formation of unstable SEI films.

3.2. Electrochemical characterization

Fig. 6 shows the first cycle charge/discharge profiles of the samples created by cycling at a 0.1 C-rate between the cut-off voltage of 0.005 and 2 V. The charge/discharge test was conducted at a constant current density of 168 $mA\,g^{-1}$. The first discharge capacities of samples AG/C, AG/C/Si, and PAA-coated AG/C/Si were approximately 329.2, 475.6, and 448.3 $mAh\,g^{-1}$, respectively. Large irreversible capacities of approximately 95.1 $mAh\,g^{-1}$ appeared in the first cycle for sample AG/C/Si. This can be attributed to the formation of a larger solid electrolyte interface (SEI) layer. Grinding the AG/C/Si composite revealed some silicon particles on the surface of the AG/C/Si composites. When silicon particles came in

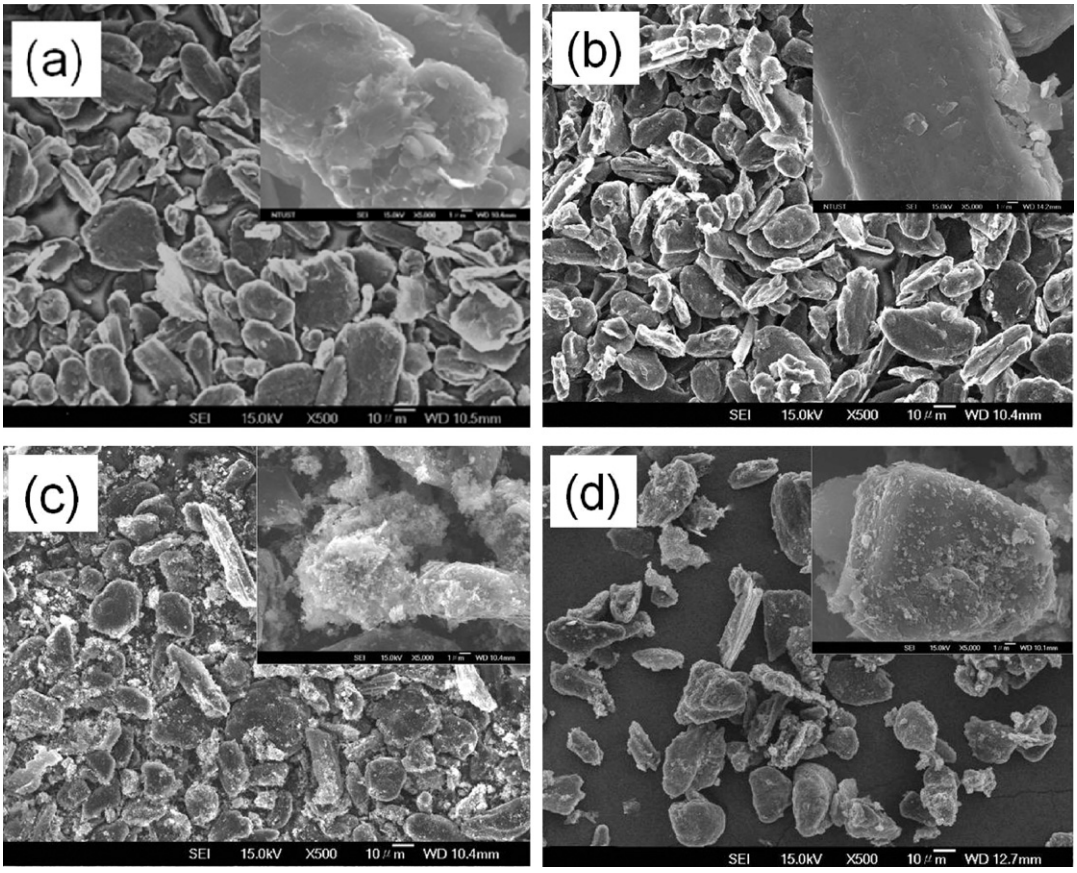

Fig. 3. FE-SEM images of (a) sample AG, (b) sample AG/C, (c) sample AG/C/Si, and (d) sample PAA-coated AG/C/Si.

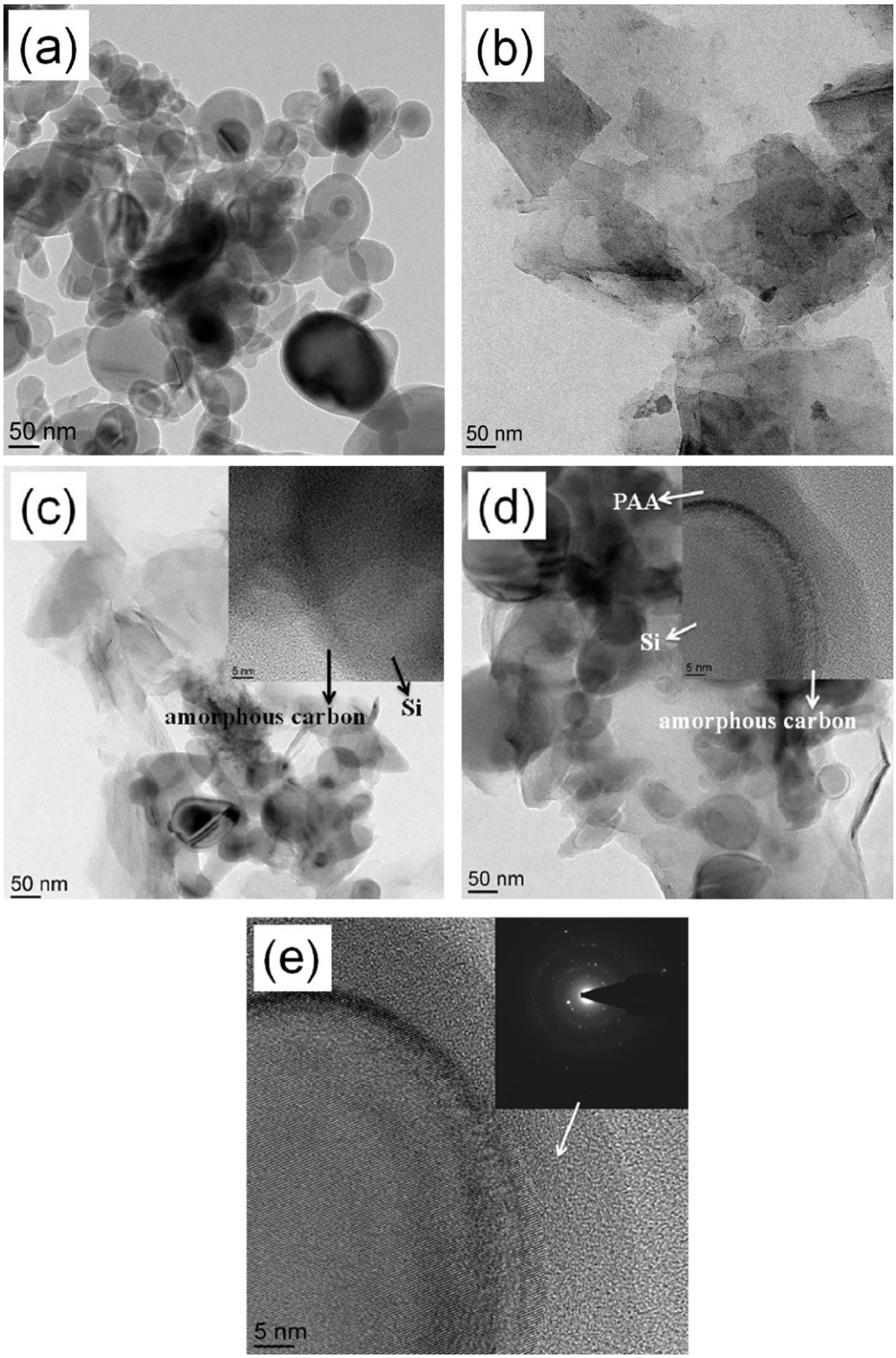

Fig. 4. TEM images of the samples: (a) nano-Si, (b) AG/C composites, (c) AG/C/Si composites, (d) PAA-coated AG/C/Si composites, and (e) selected area diffraction (SAD) patterns of PAA.

direct contact with the electrolyte, they formed unstable SEI in the silicon surface [23]. However, because PAA coating on AG/C/Si composites prevented the bare silicon from contacting the electrolyte, it formed stable SEI layers. Therefore, the first irreversible capacity decreased from 95.1 to 55.0 mAh g^{-1}. Fig. 7 plots the charge/discharge capacities of samples versus the cycle number. Sample AG/C/Si composites initially exhibited higher discharge capacities, which gradually decreased over 50 cycles. The PAA-coated AG/C/Si composite samples demonstrated cycle stability in the electrolyte solution. Table 1 shows that samples PAA-coated AG/C/Si composites had greater capacity retention than the AG/C/Si composites after 50 cycles. Because the homopolymer of

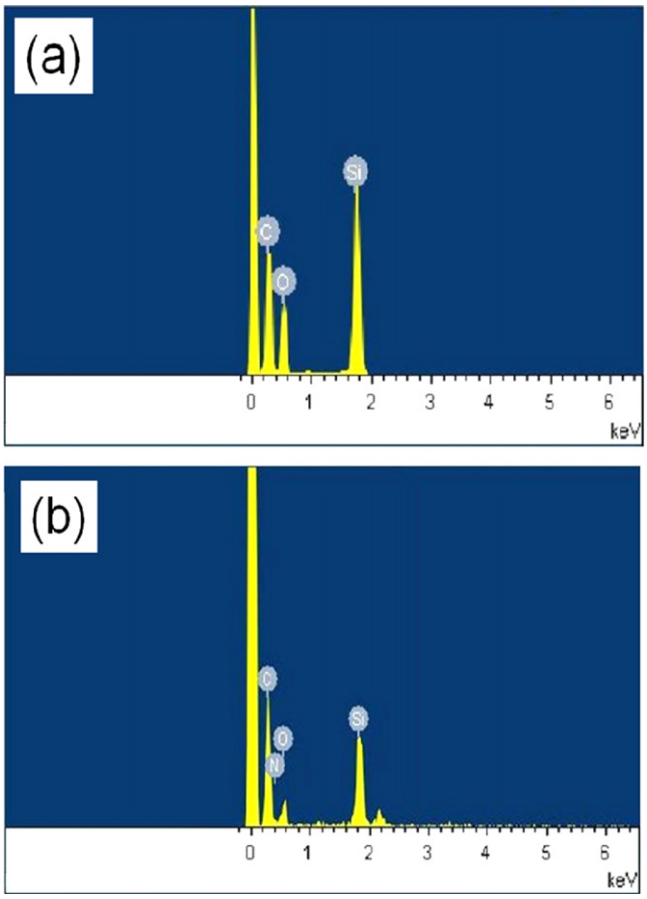

Fig. 5. EDX measurement: (a) sample AG/C/Si and (b) sample PAA-coated AG/C/Si.

2-propen-1-amine provided surface modification and an elastic network, it prevented direct material contact with the electrolyte and the silicon volume expansion caused by structure destruction (Fig. 1).

Fig. 8 displays SEM images of the morphological changes of the composite electrodes after the 50th cycle. The SEI layers formed on the AG/C electrode surface with no cracks (Fig. 8(a)). The AG/C/Si electrode surface cracked locally because of large volume change

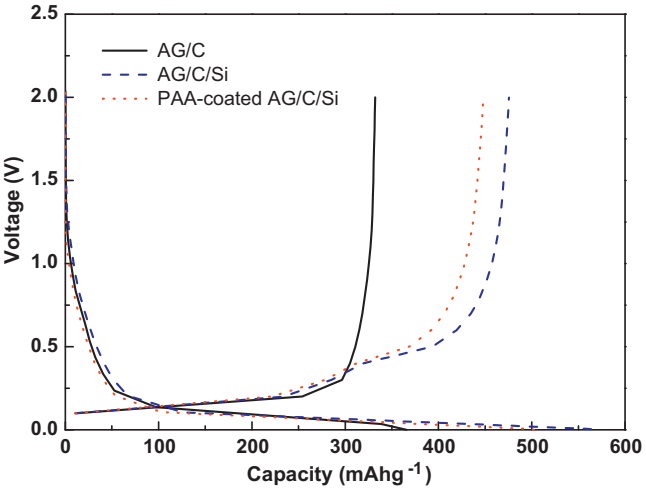

Fig. 6. The first cycle charge/discharge curves of the samples at 0.1 C between the cut-off voltage of 0.005 and 2 V (versus Li/Li^+).

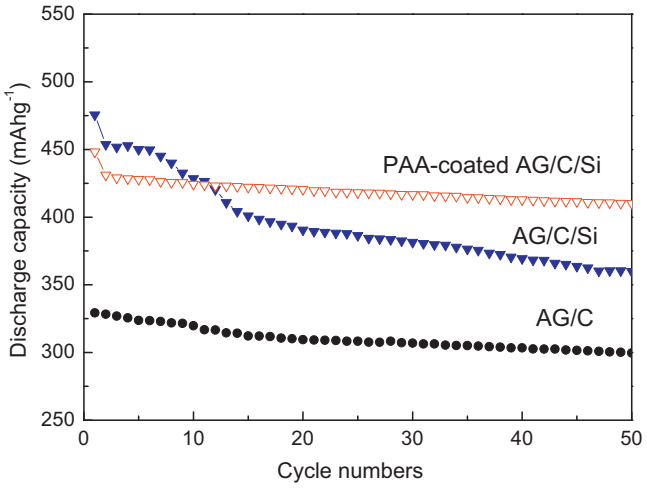

Fig. 7. Cycling performance of the samples at 0.1 C between cut-off voltages of 0.005 and 2 V (versus Li/Li^+).

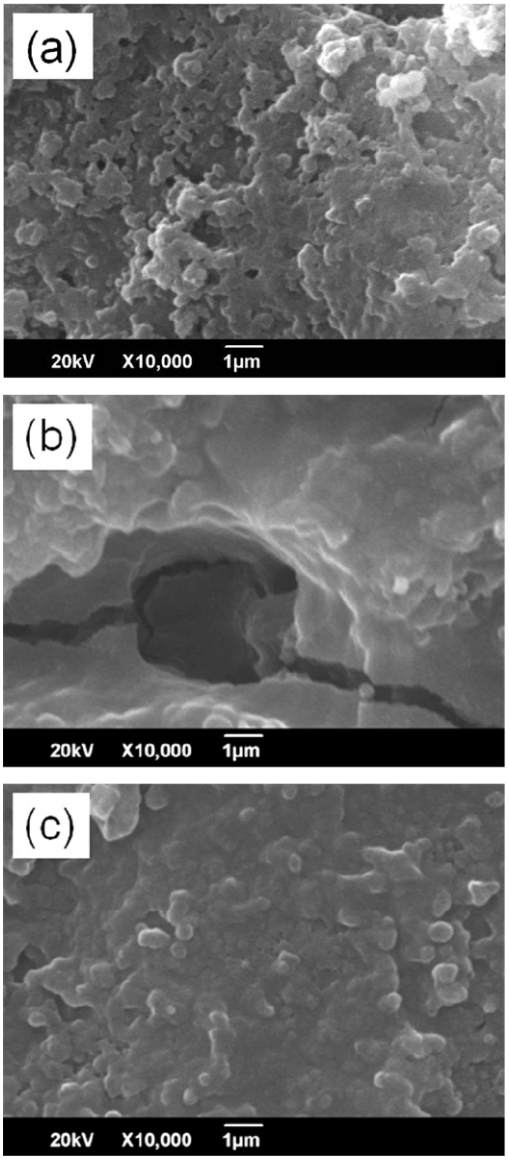

Fig. 8. SEM images of the morphological changes of the composite electrodes after 50th cycle. (a) sample AG/C, (b) sample AG/C/Si, and (c) sample PAA-coated AG/C/Si.

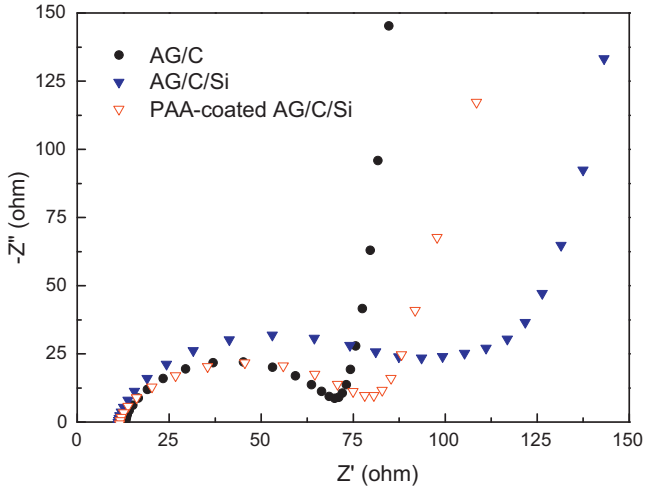

Fig. 9. The alternative current impedance spectra of the samples at open circuit potential.

(Fig. 8(b)). By contrast, the PAA-coated AG/C/Si electrode structure showed no local cracking for large volume changes (Fig. 8(c)).

Fig. 9 illustrates the alternative current impedance spectra of the samples at open circuit potential. The impedance profiles exhibit a semicircle in the high frequency range and a diminished semicircle in the low frequency range. The high frequency semicircle could be attributed to the formation of a SEI layer caused by the decomposition of the electrolyte solution, whereas the low frequency semicircle is due to charge transfer resistance [34]. The AG/C/Si composites demonstrated a higher interface resistance from the SEI, as confirmed by the high irreversible capacity at the first lithium insertion and extraction cycle. By contrast, the PAA-coated AG/C/Si composites demonstrated a relatively low SEI resistance and a significant decrease in the second semicircle by cycling; that is, a decrease of the charge transfer resistance by cycling. These results indicate that the addition of PAA decreased the specific surface area (BET) of the AG/C/Si composites. This, in turn, reduced the direct contact between the electrode surface and the electrolyte. By contrast, adding PAA formed more effective conductive networks in the electrode, which also improved the electronic conductivity.

4. Conclusions

A homopolymer of 2-propen-1-amine layer was successfully coated on the surface of AG/C/Si composite materials. This study also shows that PAA matrixes play crucial roles in significantly improving morphology stability. Previous studies on electrochemical characterization have shown that PAA-coated AG/C/Si composites provide a greater improvement in cycle reversibility and lower electrochemical resistance than bare PAA does.

Acknowledgements

The authors are thankful for the financial support of the National Science Council of Taiwan R.O.C under grant No. NSC 100-2221-E-157-007.

References

[1] H. Fujimoto, J. Power Sources 195 (2010) 5019–5024.
[2] M. Yoshio, H. Wang, K. Fukuda, T. Umeno, T. Abe, Z. Ogumi, J. Mater. Chem. 14 (2004) 1754–1758.
[3] P. Gu, R. Cai, Y. Zhou, Z. Shao, Electrochim. Acta 55 (2010) 3876–3883.
[4] Y. Zheng, J. Yang, J. Wang, Y. NuLi, Electrochim. Acta 52 (2007) 5863–5867.
[5] S. Kalnaus, K. Rhodes, C. Daniel, J. Power Sources 196 (2011) 8116–8124.
[6] C.C. Nguyen, S.W. Song, Electrochim. Acta 55 (2010) 3026–3033.
[7] L.B. Chen, J.Y. Xie, H.C. Yu, T.H. Wang, Electrochim. Acta 53 (2008) 8149–8153.
[8] X. Wang, Z. Wen, Y. Liu, Y. Huang, T.L. Wen, Solid State Ionics 192 (2011) 330–334.
[9] X. Wang, Z. Wen, Y. Liu, Electrochim. Acta 56 (2011) 1512–1517.
[10] H. Xiang, K. Zhang, G. Ji, J.Y. Lee, C. Zou, X. Chen, J. Wu, Carbon 49 (2011) 1787–1796.
[11] Z. Zhou, Y. Xu, W. Liu, L. Niu, J. Alloys Compd. 493 (2010) 636–639.
[12] X. Yang, Z. Wen, L. Zhang, M. You, J. Alloys Compd. 464 (2008) 265–269.
[13] M. Holzapfel, H. Buqa, L.J. Hardwick, M. Hahn, A. Würsig, W. Scheifele, P. Novák, R. Kötz, C. Veit, F.M. Petrat, Electrochim. Acta 52 (2006) 973–978.
[14] G.X. Wang, J.H. Ahn, J. Yao, S. Bewlay, H.K. Liu, Electrochem. Commun. 6 (2004) 689–692.
[15] M. Au, Y. He, Y. Zhao, H. Ghassemi, R.S. Yassar, B. Garcia-Diaz, T. Adams, J. Power Sources 196 (2011) 9640–9647.
[16] R. Lv, J. Yang, P. Gao, Y. NuLi, J. Wang, J. Alloys Compd. 490 (2010) 84–87.
[17] W. Zhou, S. Upreti, M.S. Whittingham, Electrochem. Commun. 13 (2011) 1102–1104.
[18] W. Zhou, S. Upreti, M.S. Whittingham, Electrochem. Commun. 13 (2011) 158–161.
[19] X. Yang, Z. Wen, X. Xu, B. Lin, S. Huang, J. Power Sources 164 (2007) 880–884.
[20] Z. Zhou, Y. Xu, M. Hojamberdiev, W. Liu, J. Wang, J. Alloys Compd. 507 (2010) 309–311.
[21] Y.N. Jo, Y. Kim, J.S. Kim, J.H. Song, K.J. Kim, C.Y. Kwag, D.J. Lee, C.W. Park, Y.J. Kim, J. Power Sources 195 (2010) 6031–6036.
[22] L. Wang, C.X. Ding, L.C. Zhang, H.W. Xu, D.W. Zhang, T. Cheng, C.H. Chen, J. Power Sources 195 (2010) 5052–5056.
[23] Q. Si, K. Hanai, T. Ichikawa, A. Hirano, N. Imanishi, Y. Takeda, J. Power Sources 195 (2010) 1720–1725.
[24] X. Yang, P. Zhang, Z. Wen, L. Zhang, J. Alloys Compd. 496 (2010) 403–406.
[25] W. Wang, P.N. Kumta, J. Power Sources 172 (2007) 650–658.
[26] H. Fukui, H. Ohsuka, T. Hino, K. Kanamura, J. Power Sources 196 (2011) 371–378.
[27] B. Fuchsbichler, C. Stangl, H. Kren, F. Uhlig, S. Koller, J. Power Sources 196 (2011) 2889–2892.
[28] J. Guo, A. Sun, X. Chen, C. Wang, A. Manivannan, Electrochim. Acta 56 (2011) 3981–3987.
[29] P. Zuo, G. Yin, Z. Yang, Z. Wang, X. Cheng, D. Jia, C. Du, Mater. Chem. Phys. 115 (2009) 757–760.
[30] Y.S. Wu, Y.H. Lee, Y.L. Tsai, J. Mater. Process. Technol. 208 (2008) 35–41.
[31] Z.Y. Zeng, J.P. Tu, Y.Z. Yang, J.Y. Xiang, X.H. Huang, F. Mao, M. Ma, Electrochim. Acta 53 (2008) 2724–2728.
[32] S.Y. Chew, Z.P. Guo, J.Z. Wang, J. Chen, P. Munroe, S.H. Ng, L. Zhao, H.K. Liu, Electrochem. Commun. 9 (2007) 941–946.
[33] Y. Zhang, Z.W. Fu, Q.Z. Qin, Electrochem. Commun. 6 (2004) 484–491.
[34] D. Aurbacha, B. Markovskya, I. Weissmana, E. Levia, Y. Ein-Eli, Electrochim. Acta 45 (1999) 67–86.